UWB Positioning Using Known Indoor Features - Environment Comparison

Jan Kietlinski-Zaleski*, Takaya Yamazato**
*School of Engineering, Nagoya University, Nagoya, Japan. Email: jkietlin@katayama.nuee.nagoya-u.ac.jp
**School of Engineering, Nagoya University, Nagoya, Japan. Email: yamazato@nagoya-u.jp

***Abstract*—Ultra-Wideband is an attractive technology for short range positioning, especially indoors. However, for normal Time of Arrival (TOA) positioning, at least three receivers with unblocked direct path to the transmitter are required. A requirement that is not always met. In our previous work [1] we presented a novel 3D TOA UWB indoor positioning method that uses only two receivers. This is possible by exploiting the knowledge of some of the indoor features, namely ceiling and walls. In this work, we verify the usability of the method using measurement results in three environments: a lecture room, a cluttered laboratory and a corridor. By comparing the results of the method for three environments, we draw conclusions about its strengths and weaknesses.**

I. Introduction

One of the important applications of ultra-wideband (UWB) technology is high precision indoor positioning. The indoor environment is characterized by strong multi-path interference, caused by a big number of reflections and diffractions. One way of coping with multi-path interference is using signals with high bandwidth. Furthermore, signal's high bandwidth translates into good time resolution, which in turn implies good accuracy of time-based ranging. Thus, UWB technology, using ultra high bandwidth signals, is very well suited for high precision, indoor positioning. UWB positioning has many possible applications, for example, in-building goods tracking, workers tracking or access control[2].

Three Dimensional (3D) Time of Arrival (TOA) Positioning using ranges to three or more receivers has been widely researched [3]. However, to date, 3D positioning using ranges to only two receivers has not been well studied. In our research, we aim to develop 3D positioning methods for lower than the conventional minimal number of receivers. In order to do that, our approach uses the later arriving multi-path components(MPCs) in the received waveform, together with the knowledge of big flat reflective surfaces in the environment. Time resolution of UWB signal is high enough to distinguish not only the direct-path signal, but also later arriving MPCs. MPCs are largely caused by reflections and diffractions from indoor features, furniture or people. Indoor features usually include big, flat reflective surfaces, ceilings and walls, subsequently called reflectors. MPCs caused by reflections from the reflectors can be used for positioning. To our knowledge, such usage of later arriving MPCs for TOA was not reported in the literature to date.

978-1-4244-5864-6/10$26.00 © IEEE

In this paper, we verify our Reflection-Aided Maximum Likelihood(RAML) method presented in [1], using the results obtained in a measurement campaign. The measurements were performed in three rooms: a lecture room, a cluttered laboratory and a corridor. RAML method results for the three environments and two different receiver arrangements are presented. The results are then used to draw conclusions about strengths and weaknesses of the method.

The rest of the paper is organized as follows: Section II presents the description of the RAML positioning method. In Section III, the details of the measurement setup are presented. Next, in IV, the characteristics of each of the environments are presented. Results of RAML method are shown and discussed in section V. Finally, conclusions are drawn in Section VI.

II. RAML 3D Two Receiver Positioning Method

In this section, a description of Reflection-Aided Maximum Likelihood(RAML) method is introduced. RAML method was first presented in [1]. However, the description presented here has been updated for clarity.

A. Motivation For The New Method

Consider a system with a mobile UWB transmitter synchronized with a set of N stationary receivers $\mathcal{R} = \{\mathrm{R}_1, \ldots, \mathrm{R}_N\}$. Let $\mathbf{b} = [x_b\ y_b\ z_b]^T$ be the unknown position of the transmitter and $\mathbf{r}_n = [x_n\ y_n\ z_n]^T, n \in \{1, \ldots, N\}$ be the known position of R_n. The superscript "T" stands for transpose.

Let $\mathbf{d}^1 = [\hat{d}_1^1\ \cdots\ \hat{d}_N^1]^T$ be a vector of the estimated direct-path ranges, from the transmitter to all $\mathrm{R}_n \in \mathcal{R}$. Position of the transmitter, $\mathbf{b}$, can be estimated by solving a set of quadratic equations:

$$\begin{cases} (x_b - x_1)^2 + (y_b - y_1)^2 + (z_b - z_1)^2 = \hat{d}_1^{1\,2} \\ \qquad\qquad \vdots \\ (x_b - x_N)^2 + (y_b - y_N)^2 + (z_b - z_N)^2 = \hat{d}_N^{1\,2} \end{cases} \tag{1}$$

For $N > 3$ a data fusion method, simplest being Least Squares, can be used. For $N = 3$ the set can be solved directly.

However, if there are only two receivers available, a direct solution is not possible. The conventional solution to finding position with only two receivers, proposed for example in [4], is to reduce the problem to 2D by assuming the height coordinate. This method performs well if the assumption is correct. However, if the assumption is not correct, the result can have a large error, both when 3D or 2D position is considered.

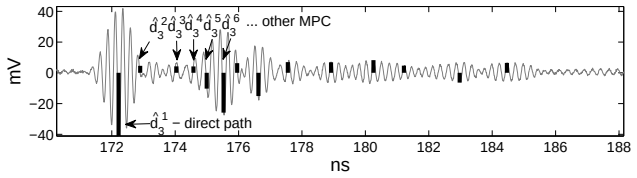

Fig. 1. Example waveform recorded at R_2 during the lecture room measurements (see Fig. 13). Black bars mark detected MPCs. $\hat{d}_3^j$ are MPC ranges of those MPCs. CLEAN algorithm (see Section III) was used for detection.

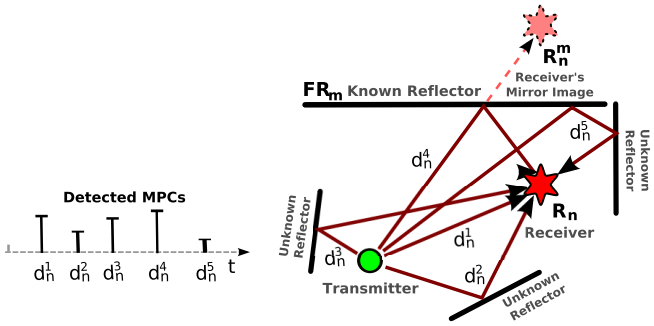

Fig. 2. Example - 5 MPC ranges $[\hat{d}_n^1 \ \cdots \ \hat{d}_n^5]^T$ are detected at receiver R_n. In LOS conditions first range matches the direct path. Problem - Which range matches the $\mathrm{FR_m}$-reflected path?

In order to avoid this large error, more information is needed to achieve a better transmitter position estimate. In the RAML method, all detected MPCs and the knowledge of big, flat reflective surfaces in the environment are used to provide this information. Fig. 1 presents an example received waveform. Due to UWB's high time resolution, some MPCs in the waveform are resolvable. MPCs detected using CLEAN algorithm (see Section III) are marked with black bars. If, considering one reflector-receiver pair, it was known which detected MPC in the received waveform matches the reflection from the reflector, using this MPC for positioning would be relatively easy. In an example shown in Fig. 2, 5 MPCs with ranges $[\hat{d}_n^1 \ \cdots \ \hat{d}_n^5]^T$ are detected in the received waveform. First range, $\hat{d}_n^1$, will, in LOS conditions, correspond to direct path, making it useful for positioning. If it is known that $\hat{d}_n^4$ MPC range corresponds to reflection from FR_m reflector, $\hat{d}_n^4$ can also be useful. $\hat{d}_n^4$ can be used as an additional range measurement to R_n^m, the mirror image of the real receiver through reflector. However, in reality, it is not known which MPC matches the reflection. In the example, it could be any of the detected MPCs, including MPCs caused by the three unknown reflectors, but also direct-path $\hat{d}_n^1$. The RAML method concentrates on using information contained in MPCs while solving the above-mentioned problem, assuming that for each reflector-receiver pair the probability of a matching MPC existing is high.

B. System Model

This section defines the terms used in the method description. The terms include system components: transmitter, receivers, reflectors; as well as the terms used to describe MPCs in the received waveforms.

Consider a system with a mobile UWB transmitter synchronized with a set of N stationary receivers $\mathcal{R}$, as already mentioned in Section II-A. Transmitter transmits a pulse waveform received by $\mathrm{R}_n \in \mathcal{R}$. Waveform received by R_n is often represented in the literature as:

$$r_n(t) = \sum_{k=1}^{K_n} \alpha_n^k s(t - \tau_n^k) + e_n(t), \tag{2}$$

where K_n is the number of MPCs, α_n^k and τ_n^k are the fading coefficient and delay of k_{th} MPC, respectively, $e_n(t)$ is a zero-mean additive white Gaussian noise (AWGN) and $s(t)$ is the transmitted pulse waveform. Subscript n is the receiver number to which the parameter applies.

The position of transmitter, $\mathbf{b}$, is considered to be inside Service Area SA, defined by vector $[x_{min} \ y_{min} \ z_{min} \ x_{max} \ y_{max} \ z_{max}]^T$.

$$\mathbf{b} \in \mathrm{SA} \Leftrightarrow \begin{array}{l} x_{min} \le x_b \le x_{max} \\ y_{min} \le y_b \le y_{max} \\ z_{min} \le z_b \le z_{max} \end{array} \tag{3}$$

The transmitter position probability distribution in SA is considered to be unknown.

Let $\mathcal{FR} = \{\mathrm{FR}_1, \cdots, \mathrm{FR}_M\}$ be a set of known M big, flat reflective surfaces, for example ceiling and walls. Each reflector FR_m is defined by roughness $\sigma^2_{\mathrm{FR}_m}$ and a 3D surface equation:

$$\begin{array}{l} A_m x + B_m y + C_m z + D_m = 0 \\ \sqrt{A_m^2 + B_m^2 + C_m^2} = 1 \end{array} \tag{4}$$

where $[A_m \ B_m \ C_m \ D_m]^T$ are normalized surface coefficients of FR_m and $[x \ y \ z]^T$ are coordinates in 3D space. Roughness $\sigma^2_{\mathrm{FR}_m}$ is the MPC range variance caused by reflection from FR_m. $\sigma^2_{\mathrm{FR}_m}$ models the error in reflector position and the influence of the irregularities of the reflector.

A FR_m-reflected path between the transmitter and R_n can be represented by a direct path between the transmitter and R_n's mirror image through FR_m. Let R_n^m designate the mirror image of R_n through FR_m. In addition, let $\mathbf{r}_n^m = [x_n^m \ y_n^m \ z_n^m]^T$ designate the position of R_n^m. $\mathbf{r}_n^m$ can be calculated as:

$$\mathbf{r}_n^m = \mathbf{r}_n - 2\Big(\mathbf{r}_n \cdot \begin{bmatrix} A_m \\ B_m \\ C_m \end{bmatrix} + D_m\Big) \begin{bmatrix} A_m \\ B_m \\ C_m \end{bmatrix} \tag{5}$$

where "$\cdot$" is the scalar product and $[A_m \ B_m \ C_m]^T$ is the normal vector of FR_m.

For positioning, MPC ranges, ranges corresponding to each detected MPC delay, are used. In the ranging step, each receiver R_n can detect not only first, but all distinct MPCs in the received waveform. For each R_n, the intermediate result is a vector of J_n detected MPC delay estimates $\tau_n = [\hat{\tau}_n^1 \ldots \hat{\tau}_n^{J_n}]^T$. $\hat{\tau}_n^j$ is assumed to have a Gaussian error distribution. Assuming

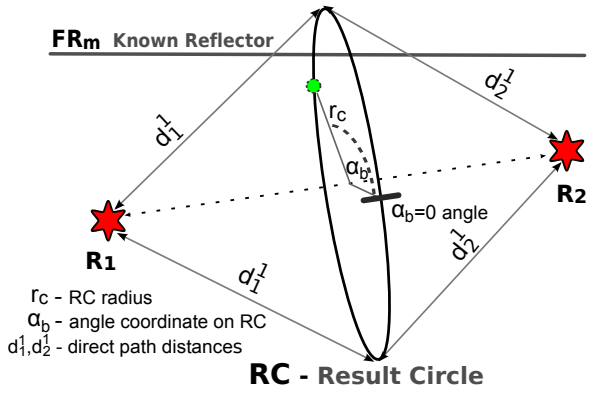

Fig. 3. Result Circle - locus of points at a range of $\hat{d}_1^1$ from R_1 and $\hat{d}_2^1$ from R_2. Point's position on RC is described by $\alpha_b r_c$.

free space propagation, a vector of MPC range estimates $\mathbf{d}_n = [\hat{d}_n^1 \cdots \hat{d}_n^{J_n}]^T$ is calculated as:

$$\hat{d}_n^j = \hat{\tau}_n^j C, \quad j = 1, \ldots, J_n \tag{6}$$

where C is the speed of light and $\hat{d}_n^j$ is also assumed to have a Gaussian distribution: $\hat{d}_n^j = d_n^j + e_n^j \sim N(0, {\sigma_n^j}^2)$.

C. RAML Method's Algorithm

In this section we present the algorithm of RAML method. The method is divided into two steps. The first step consists of using positions of two receivers ($\mathbf{r}_1$, $\mathbf{r}_2$) and detected direct ranges ($\hat{d}_1^1$, $\hat{d}_2^1$) for finding the RC. The position of the transmitter is assumed to be near RC. The second step consists of calculating a likelihood function for points on the RC using the knowledge of all detected MPCs ($\mathbf{d}_1$, $\mathbf{d}_2$), $\mathcal{FR}$ and SA. The point on RC with maximum likelihood is chosen as the estimated transmitter position.

1) Result Circle (RC): If direct range estimates to only two receivers are available, equation set (1) becomes:

$$\begin{cases} (x_b - x_1)^2 + (y_b - y_1)^2 + (z_b - z_1)^2 = {\hat{d}_1^1}^2 \\ (x_b - x_2)^2 + (y_b - y_2)^2 + (z_b - z_2)^2 = {\hat{d}_2^1}^2 \end{cases} \tag{7}$$

The solution of (7) is, in a non-degenerate case, a 3D circle. Let the circle be designated as Result Circle (RC). An example RC is shown in Fig. 3. A reference zero angle is marked. Assuming small direct-path range estimate errors ($\hat{d}_1^1$, $\hat{d}_2^1$), the transmitter is near the RC. The transmitter position estimate will be chosen from points on the RC, $\hat{\mathbf{b}} \in \mathrm{RC}$. Transmitter is also considered to be inside SA, therefore $\hat{\mathbf{b}} \in \mathrm{SA} \cap \mathrm{RC}$.

The RC can be described with radius r_c and transformation $Q(\cdot)$, where $Q(\cdot)$ is a translation plus rotation that moves a flat($z_b' = 0$) 2D circle of radius r_c centered at $[0\ 0\ 0]^T$ from XY plane to RC's position. A point on the RC can be described as a function of, equivalently, either angle α_b or arc (radius times angle) $r_c\alpha_b$, from a chosen $\alpha_b = 0$ reference. Arc is used because it is also used in the method's implementation. Since the point is a transmitter position estimate candidate, it will be denoted as $\hat{\mathbf{b}}(r_c\alpha_b) = [x_b\ y_b\ z_b]^T$. $\hat{\mathbf{b}}(r_c\alpha_b)$ for a given $r_c\alpha_b$ can be calculated as:

$$\begin{cases} x_b' = r_c \cos\alpha_b \\ y_b' = r_c \sin\alpha_b \\ z_b' = 0 \end{cases}, \hat{\mathbf{b}}(r_c\alpha_b) = Q\Big(\begin{bmatrix} x_b' \\ y_b' \\ z_b' \end{bmatrix} \Big) \tag{8}$$

where $\hat{\mathbf{b}}' = [x_b'\ y_b'\ z_b']^T$ is the point's position on the RC in the prime base, before $Q(\cdot)$ transformation, while $\hat{\mathbf{b}}(r_c\alpha_b)$ is point's position after RC is moved to its actual location. Only $r_c\alpha_t : \hat{\mathbf{b}}(r_c\alpha_b) \in SA$, are considered.

2) Position on RC Calculation: The second step of the RAML method consists of finding the best transmitter position estimate on the RC, $\hat{\mathbf{b}}(r_c\alpha_b)$. To accomplish this, maximum likelihood estimator using later detected MPCs ($\mathbf{d_1}$, $\mathbf{d_2}$) and knowledge of $\mathcal{FR}$ is used.

Instead of considering $\mathcal{R}$, $\mathcal{FR}$, $\mathbf{d_1}$ and $\mathbf{d_2}$ together, the problem can be divided, with each $(\mathrm{R}_n, \mathrm{FR}_m) \in \mathcal{R} \times \mathcal{FR}$ pair being considered separately. "$\times$" here is the Cartesian product. The result for each pair is a partial likelihood function defined for $\hat{\mathbf{b}} \in \mathrm{SA} \cap \mathrm{RC}$, $L_n^m(\mathbf{d_n}; r_c\alpha_b)$. Functions for each pair can then be combined for a final result. A $(\mathrm{R}_n, \mathrm{FR}_m)$ pair represents a FR_m-reflected path from transmitter to R_n. As mentioned in Section II-B, this path can be also represented with a direct path from transmitter to R_n^m, R_n's reflection through FR_m.

3) Partial Likelihood Function Derivation: As the first approach, let $\hat{d}_n^j$ be a known a priori MPC range matching the FR_m-reflected path to R_n. This assumption is for explanation purposes only, since it is not true for the RAML method. Let $d_{(n,m)}$ be the real FR_m-reflected path length to R_n, of which $\hat{d}_n^j$ is an estimate. If $\hat{d}_n^j$ error is assumed to be Gaussian, $\hat{d}_n^j \sim N(d_{(n,m)}, {\sigma_n^j}^2 + {\sigma_{\mathrm{FR}_m}}^2)$, the likelihood function is:

$$L_n^m(\hat{d}_n^j; d_{(n,m)}) = N_{\mathrm{rm}} \exp\left(\frac{-1}{2} \frac{(d_{(n,m)} - \hat{d}_n^j)^2}{{\sigma_n^j}^2 + {\sigma_{\mathrm{FR}_m}}^2} \right) \tag{9}$$

where N_{rm} is a normalization constant, and exp is the exponential function. $L_n^m(\hat{d}_n^j; d_{(n,m)})$ should be considered as a function of $d_{(n,m)}$. $L_n^m(\hat{d}_n^j; d_{(n,m)})$ is a Gaussian function centered at $\hat{d}_n^j$. This result is understandable since this simple case corresponds to having one direct-path range estimate to R_n^m.

In practice, there is no a priori knowledge about FR_m-MPC matches. Any detected MPC range may match $d_{(n,m)}$. Additionally, the matching MPC range is not always detected and present in $\mathbf{d}_n$. Considering those two problems, a more realistic $d_{(n,m)}$ likelihood function can be constructed as:

$$L_n^m(\mathbf{d_n}; d_{(n,m)}) = N_{\mathrm{rm}} \left(P_{\mathrm{ndet}} + \sum_{j=1}^{J_n} P_j \exp\left(\frac{-1}{2} \frac{(d_{(n,m)} - \hat{d}_n^j)^2}{{\sigma_n^j}^2 + {\sigma_{\mathrm{FR}_m}}^2} \right) \right)$$
$$P_1 = P_{\mathrm{fst}}\ ,\ P_j \overset{j \in [2 \cdots J_n]}{=} 1 \tag{10}$$

where P_{ndet} represents the chance that the matching MPC range was not detected, J_n is number of detected MPCs, $\hat{d}_n^j$ is the j_{th} MPC range estimate. Instead of one Gaussian function in (9), (10) is a sum of Gaussian functions, each representing

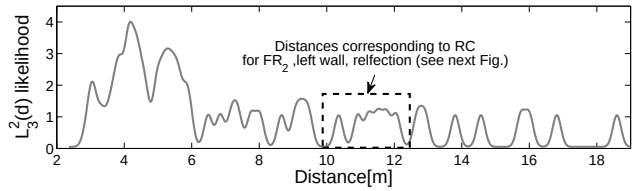

Fig. 4. Example $L_n^m(\mathbf{d}_n; d)$ partial likelihood function plotted as a function of range from $\mathrm{R}_\mathrm{n}^\mathrm{m}$. Measurement data for $\mathrm{B_{REF}}$ and R_2 are used (see Fig. 13). N_rm is set to 1(see Eq. (10)).

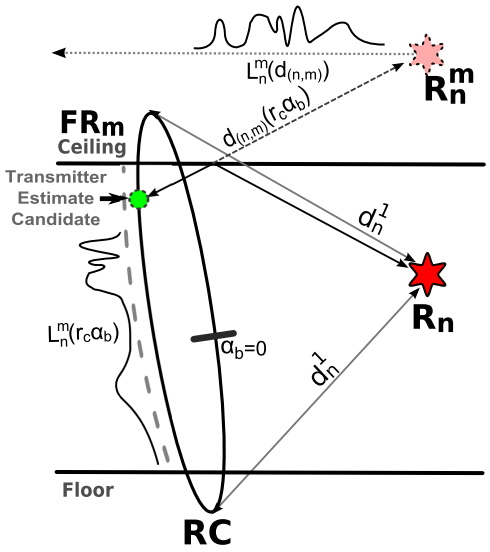

Fig. 5. Two partial likelihood functions, $L_n^m(\mathbf{d_n}; d_{(n,m)})$ and $L_n^m(\mathbf{d_n}; r_c\alpha_b)$, for one $\mathrm{R_n}$-$\mathrm{FR_m}$ pair. $L_n^m(\mathbf{d}_n; d_{(n,m)})$ is a function of range from $\mathrm{R}_\mathrm{n}^\mathrm{m}$. $L_n^m(\mathbf{d}_n; r_c\alpha_b)$ is a function of position on RC.

the likelihood of $d_{(n,m)}$ being near to one $\hat{d}_n^j$. The contribution of the first MPC range, direct-path range, P_1 is set lower to P_fst to offset the tendency of the algorithm to assign high likelihood directly near the reflector FR_m. An example $L_n^m(\mathbf{d}_n; d_{(n,m)})$ plotted against $d_{(n,m)}$ is presented in Fig. 4. As noted on the figure, only a small interval of $d_{(n,m)}$ values corresponds to points on the RC.

The two previous paragraphs discussed likelihood functions of the reflected path length $d_{(n,m)}$. However, the function of real interest is $L_n^m(\mathbf{d}_n; r_c\alpha_b)$, the likelihood function defined for $\hat{\mathbf{b}}(r_c\alpha_b)$, points on RC. Equation (4) can be changed to a function of $r_c\alpha_b$ by replacing $d_{(n,m)}$ with range between

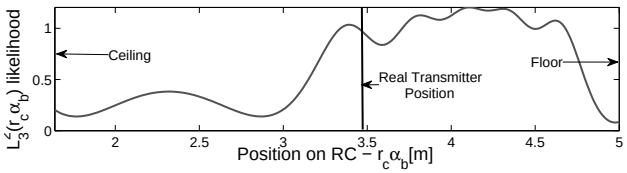

Fig. 6. $L_n^m(\mathbf{d}_n; r_c\alpha_b)$ partial likelihood function plotted as a function of position on RC. Only positions on an arc inside SA are considered. Measurement data for $\mathrm{B_{REF}}$ and R_2 are used (see Fig. 13). Reflector FR_2, left wall, is considered.

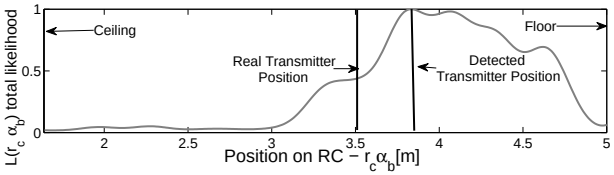

Fig. 7. $L(\mathbf{d}_n; r_c\alpha_b)$ total likelihood function plotted as a function of position on RC. Measurement data for $\mathrm{B_{REF}}$ are used (see Fig. 13).

reflected receiver R_n^m and the point, $|\mathbf{r}_n^m - \hat{\mathbf{b}}(r_c\alpha_b)|$:

$$L_n^m(\mathbf{d_n}; r_c\alpha_b) = N_\mathrm{rm}\left(P_\mathrm{ndet} + \sum_{j=1}^{J_n} P_j \exp\left(\frac{-1}{2}\frac{(|\mathbf{r}_n^m - \hat{\mathbf{b}}(r_c\alpha_b)| - \hat{d}_n^j)^2}{{\sigma_n^j}^2 + {\sigma_{\mathrm{FR}_m}}^2}\right)\right) \quad (11)$$

Fig. 5 illustrates the connection between $L_n^m(\mathbf{d}_n; d_{(n,m)})$ and $L_n^m(\mathbf{d}_n; r_c\alpha_b)$. Fig. 6 presents an example of $L_n^m(\mathbf{d}_n; r_c\alpha_b)$. In this case, $\mathrm{RC} \cap \mathrm{SA}$, the domain of $L_n^m(\mathbf{d}_n; r_c\alpha_b)$, is an arc from the ceiling to the floor.

4) Combining Likelihood Functions: After calculating partial likelihood functions for each $(\mathrm{R}_n, \mathrm{FR}_m) \in \mathcal{R} \times \mathcal{FR}$ pair, the total likelihood function $L(r_c\alpha_b)$ can be calculated. As can be seen in Fig. 6, partial results for one $(\mathrm{R}_n, \mathrm{FR}_m)$ pair does not usually provide a good position estimate. However, if probability of not detecting a matching MPC is low, $L_n^m(\mathbf{d}_n; r_c\alpha_b)$ likelihood for most $(\mathrm{R}_n, \mathrm{FR}_m)$ pairs will be high for $r_c\alpha_b$ corresponding to the best transmitter position estimate $\hat{\mathbf{b}}(r_c\alpha_b)$. Consequently, total likelihood for $\hat{\mathbf{b}}(r_c\alpha_b)$ should also be high. If $L_n^m(\mathbf{d}_n; r_c\alpha_b)$ are mutually independent, the total likelihood function can be calculated as:

$$L(r_c\alpha_b) = \prod_{n\in[1,N], m\in[1,M]} L_n^m(r_c\alpha_b) \quad (12)$$

Assumption of the independence of $L_n^m(\mathbf{d}_n; r_c\alpha_b)$ is not strictly correct, but the introduced error is small. Example of the total likelihood function $L(r_c\alpha_t)$, for the same transmitter as before, is presented in Fig. 7.

Finally, $r_c\alpha_t$ estimate can be found by maximizing likelihood:

$$r_c\hat{\alpha}_b = \arg\max_{r_c\alpha_b}\left(\sum_{n\in[1,N], m\in[1,M]} \ln L_n^m(r_c\alpha_b)\right) \quad (13)$$

The result transmitter position estimate is $\hat{\mathbf{b}}(r_c\hat{\alpha}_b)$.

III. Measurement Setup

In this paper, we verify the usability of the RAML method using measurements performed in three different environments: a lecture room, a laboratory and a corridor. The measurements took place at Warsaw University of Technology(PW), Department of Electronics and Information Theory(EiTI), in cooperation with Dr. Jerzy Kolakowski, Radiomeasurement Laboratory. Figures 8 and 9 present the schematic and the picture of the measurement setup, respectively.

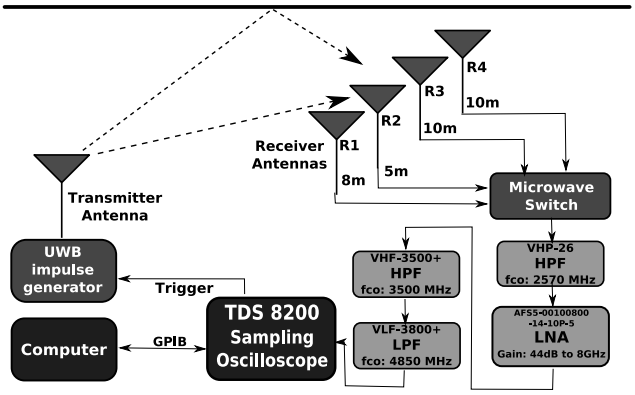

Fig. 8. Measurement Setup, schematic

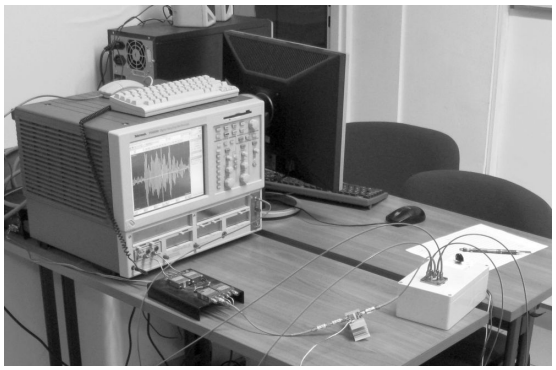

Fig. 9. Measurement Setup, picture

An Impulse Generator developed in the Radio-measurement Laboratory was used for generating the transmitted waveform. The waveform was designed for the 3.4-4.8 GHz band. Fig. 10 presents the waveform and its spectrum.

The transmitter and the receiver antennas were identical elliptic planar monopoles. Fig. 11 presents their measured radiation pattern, calculated using the waveform's amplitude.

The standard CLEAN algorithm was used for MPC detection in the received waveforms[5]. The transmitted waveform from Fig. 10 was used as the template. The algorithm stop threshold was set to $\frac{1}{10}$ of maximum MPC amplitude or $6\hat{\sigma}_e$, whichever was higher. $\hat{\sigma}_e$ is the calculated noise standard deviation after convolution with the template, calculated using a MPC-free part of the received waveform. Two additional, post-processing steps were used:

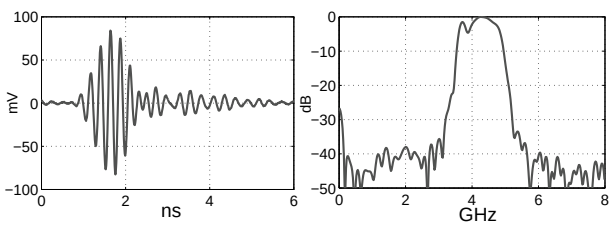

Fig. 10. Transmitted waveform, measured at antenna's input.

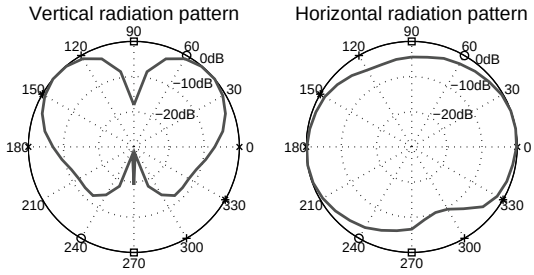

Fig. 11. Measured radiation pattern of the elliptic planar monopole antenna used.

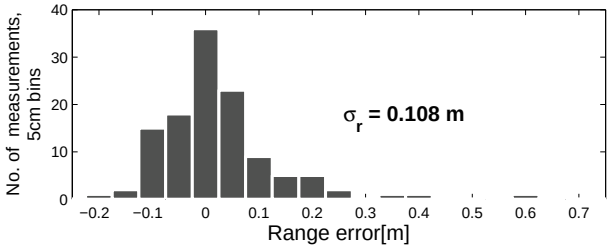

Fig. 12. Direct-path (d_n^1) ranging error histogram for lecture room, R_2 and R_3 (combined). Calculated error standard deviance is $\sigma_r = 0.108\mathrm{m}$.

1) If after the initial 1,2 or 3 MPCs there is a long pause ($>$ 5ns), those MPCs are deleted. This is to remove spurious early MPCs, caused most probably by LNA power cable acting as an antenna.
2) The threshold for the first MPC is raised to $\frac{1}{5}$ of maximum MPC amplitude. This is to combat spurious MPCs detected just before the first MPC. Those can be caused by a mismatch between the template and the real received waveforms.

Both additional steps were introduced to correct the mentioned problems, after examining the measured received waveform. The final result of the CLEAN algorithm, for one $\mathrm{R}_n \in \mathcal{R}$, is a vector of measured delays $\tau_n = [\hat{\tau}_n^1, \cdots, \hat{\tau}_n^{J_n}]^T$.

Table I presents values of parameters used in the RAML method. σ_n is the basic range error standard deviation. All σ_n^j are set to σ_n. This is a simplification, but it is not possible to know standard deviation for each MPC range. σ_n was chosen as a round number close to the direct-path error standard deviation in the lecture room environment (Error histogram shown in Fig. 12). σ_{FR_n} for each FR_n in each environment was calculated and then rounded using measurement data. Differences between the expected path length $|\mathbf{r}_n^m - \mathbf{b}|$ and closest MPC range were used. Values of P_{ndet} and P_{fst} were chosen experimentally, by finding P_{ndet} and P_{fst} delivering best results in the lecture room environment.

IV. Environment Descriptions

The measurements were performed in three environments, the lecture room, the laboratory and the corridor. In each measurement, the service area SA was considered to be the room the measurements took place in.

TABLE I
PARAMETERS USED IN THE RAML METHOD

σ_n	$0.1m$
P_{ndet}	0.05
P_{fst}	0.3

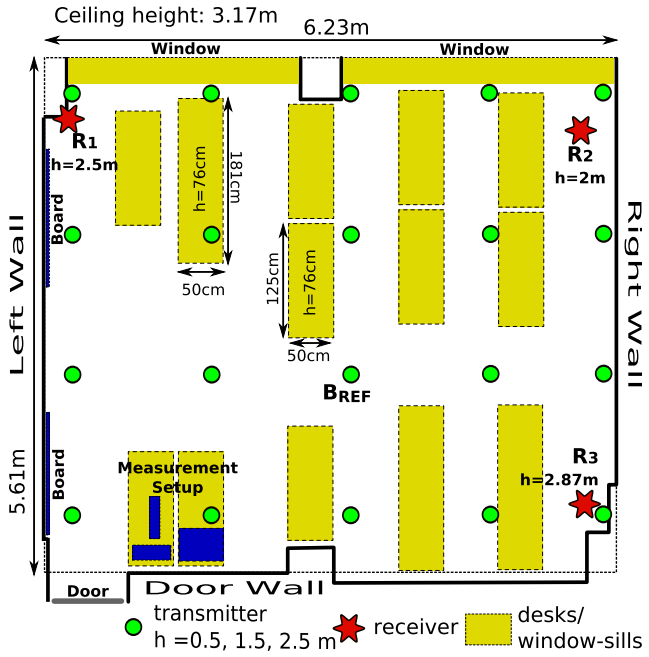

Fig. 13. Layout of the environment No.1: Lecture room

A. Lecture Room

The first environment is a typical lecture room of the EiTI department. Fig. 13 presents the environment layout. The size of the room is 6.23m by 5.61m, with ceiling at 3.17m. The room can be described as sparsely furnished.

Receiver pairs (R_2,R_3) and (R_1, R_3) were used for positioning. First pair of receivers is on the same wall (right wall), whereas receivers from the second pair are located in two corners diagonal to each other.

Measurements were performed for each of the 20 positions marked in Fig. 13, placing the transmitter at heights of 0.5m, 1.5m and 2.5m, for a total of 60 transmitter positions. To remove the effect of delays introduced by the oscilloscope, cables and receiver circuit, transmitter B_{REF} at height 1.5m was used as reference. Ceiling, floor, left wall, right wall and door wall (see Fig. 13) were used, in that order, as reflectors.

B. Laboratory

The second environment is the laboratory room of the Radio-measurement Laboratory. Fig. 14 presents the environment layout. The size of the room is 5.415m by 6.18m, with ceiling at 3.17m. The laboratory can be described as very cluttered, with measurement equipment, computers, bookshelves, metal cases etc. occupying most of the space.

Receiver pairs (R_1,R_3) and (R_2, R_3) were used for positioning. First pair of receivers is on the same wall (left wall),

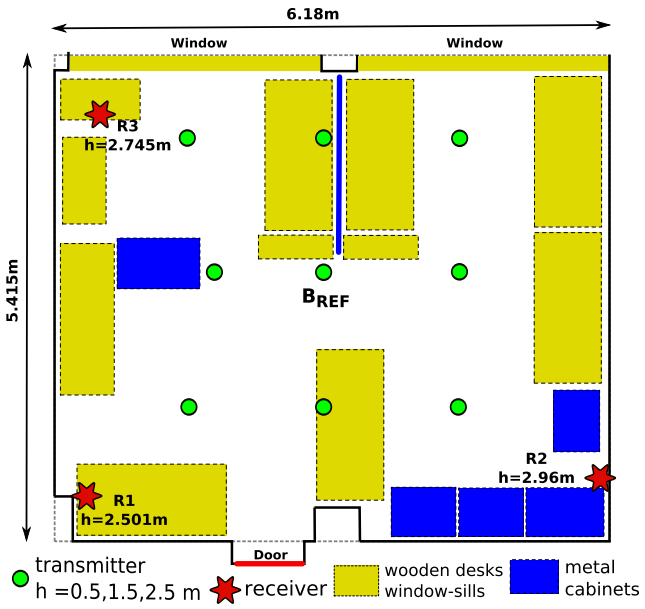

Fig. 14. Layout of the environment No.3: Laboratory

whereas receivers from the second pair are located in two corners diagonal to each other.

Measurements were performed for each of the 9 positions marked in Fig. 14, again placing the transmitter at heights of 0.5m, 1.5m and 2.5m, for a total of 27 transmitter positions. Transmitter B_{REF} at height 1.5m was used as reference. Ceiling, floor, left wall, right wall, door wall and window wall were used, in that order, as reflectors.

C. Corridor

The third environment is one of the corridors in the wings of the EiTI department. Fig. 15 presents the environment layout. The size of the corridor is 12.79m by 2.1m, with a low ceiling at 2.59m. The distinguishing feature of the corridor is its long shape. The corridor also contains metal cases that cause strong reflections. Receiver pair (R_1,R_2) was used for positioning.

Measurements were performed for each of the 11 positions marked in Fig. 15, placing the transmitter at heights of 0.5m, 1.5m and 2.3m, for a total of 33 transmitter positions. Positions along the corridor and in front of each door were chosen. Transmitter B_{REF} at height 1.5m was used as reference. Ceiling, floor, left wall and right wall were used, in that order, as reflectors.

V. MEASUREMENT RESULTS

In this section, the results of the RAML method are compared with two conventional methods, Assumed Height(AH) and Direct Solution(DS), in five different cases. The cases investigated are:

- Lecture room with receivers on one wall (R_2,R_3)
- Lecture room with diagonal receivers (R_1,R_3)
- Laboratory with receivers on one wall (R_2,R_3)
- Laboratory with diagonal receivers (R_2,R_3)
- Corridor with receivers in opposite ends

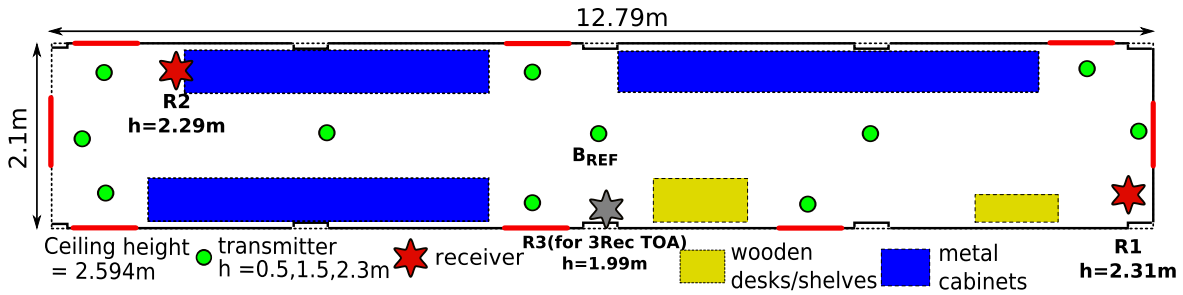

Fig. 15. Layout of the environment No.3: Corridor

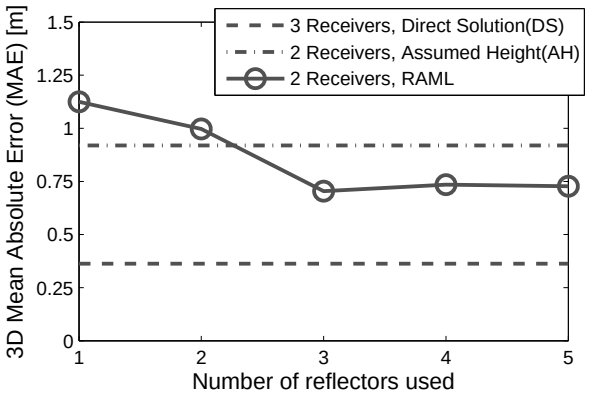

Fig. 16. Lecture room, same wall receivers- 3D MAE error versus the number of reflectors used in the method.

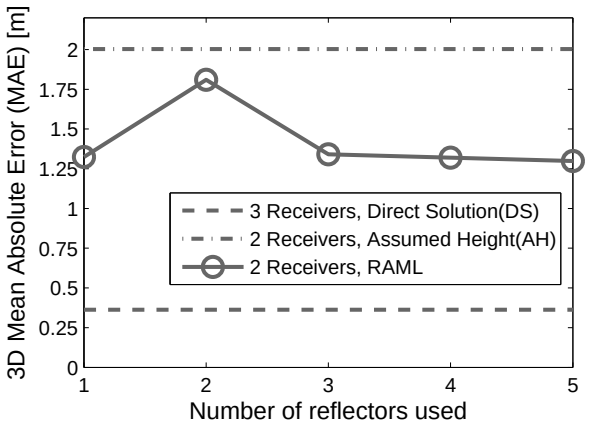

Fig. 17. Lecture room, diagonal receivers - 3D MAE error versus the number of reflectors used in the method.

3D Mean Absolute Error(MAE) metric is used. 3D MAE is calculated as an average euclidean distance between the real and estimated 3D positions of transmitters:

$$E_{3\mathrm{D}} = \frac{1}{S}\sum_{s=1}^{S}\sqrt{(\hat{x}_b^s - x_b^s)^2 + (\hat{y}_b^s - y_b^s)^2 + (\hat{z}_b^s - z_b^s)^2} \qquad (14)$$

where S is the number of transmitters, $\hat{\mathbf{b}}_s = [\hat{x}_b^s\ \hat{y}_b^s\ \hat{z}_b^s]^T$ is the transmitter's estimated position and $\mathbf{b}_s = [x_b^s\ y_b^s\ z_b^s]^T$ is the transmitter's real position. For the AH method, $\hat{z}_b^s = 1.5\mathrm{m}$ is used.

In the first case, RAML method was tested using lecture room measurements and receivers on one wall, R_2 and R_3. Results are presented in Fig. 16. The DS three receiver positioning method corresponds to directly solving equation set (1). Since DS method does not use reflectors, results for this method are independent of their number. DS method unsurprisingly achieves the lowest error. However, while being the method with lowest error, DS uses three receivers while the other two methods use only two. The AH method is the reference conventional two receiver method. In this method, the transmitter is assumed to be at the height of 1.5m, which is the average transmitter height. Like DS, AH method does not use reflectors, the method results do not depend on their number. Comparing to AH, the RAML method is more accurate when three or more reflectors are used, with MAE being around 25% lower.

It is interesting to note, that despite promising results with two and three reflectors, adding 4th and 5th reflectors did not improve the results of the RAML method. The proposed explanation is that the later two reflectors are not of the same quality as the first three (ceiling, floor and left wall). The fourth reflector is the right wall, situated directly behind the receivers. The reflections from this wall always appear very close to the first MPC, making them hard to detect. Also, the receiver antennas were positioned with the antenna's back towards the back wall, making the antenna gain very small. As can be seen in Fig. 13, 5th wall, the door wall, is uneven, with a protruding pillar and sections on either side of the pillar being of different depths, making a flat reflector a poor approximation of its shape.

In the second case, RAML method was tested using lecture room measurements and receivers in diagonal corners, R_1 and R_3. Results are presented in Fig. 17. RAML and AH methods are generally less accurate, comparing to the same wall receivers case. Also, for any number of reflectors, RAML method is more accurate than the AH method. This is caused by the fact that, contrary to the same wall receivers case, both transmitter positition candidates calculated using AH method fall into SA, or, in the case of RAML, two parts of the RC fall into SA. In the case of same wall receivers case, only one position candidate, or only one part of the RC, fell into the

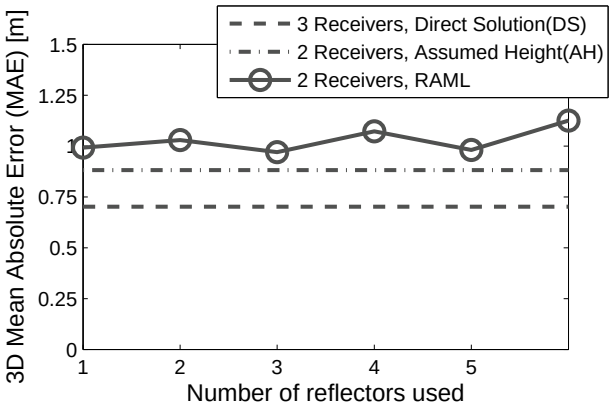

Fig. 18. Laboratory, same wall receivers - 3D MAE error versus the number of reflectors used in the method.

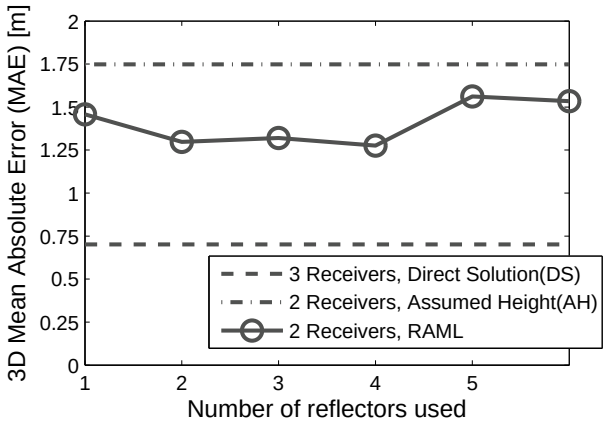

Fig. 19. Laboratory, diagonal receivers - 3D MAE error versus the number of reflectors used in the method.

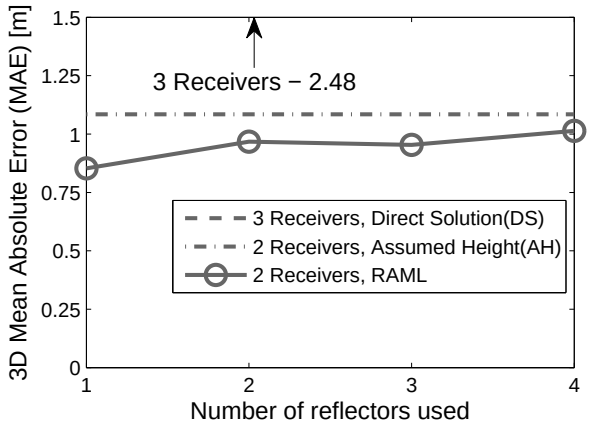

Fig. 20. Corridor, receivers at both ends - 3D MAE error versus the number of reflectors used in the method.

SA. In the AH method, one of the two position candidates has to be randomly chosen, causing a sizable error. On the other hand, in the RAML method, the method is in most cases able to correctly decide the right part of the RC the transmitter is in, limiting the error, allowing for better results than AH method. We cannot as of now explain the peak of RAML method's error at 2 reflectors. This could be caused by mistaking the reflection from the floor as a reflection from the ceiling, and vice versa, since ceiling and floor consist the first two reflectors.

In the third case, RAML method was tested using laboratory measurements and receivers on one wall, R_1 and R_3. Results are presented in Fig. 18. In this case, RAML method is less accurate than AH method for any number of reflectors. This is caused by a very cluttered nature of the environment. The equipment, shelves, metal cases etc. cause many reflections and consequently many MPCs, lowering the accuracy of the RAML method. It can also be noted that the DS method performs not as well as in the lecture room. This is caused by the direct path being blocked to some of the transmitter positions.

In the fourth case, RAML method was tested using laboratory measurements and receivers in diagonal corners, R_2 and R_3. Results are presented in Fig. 19. The RAML method is more accurate than AH method in this case. The cause is the same as in case two, diagonal receivers in a lecture room. In the presence of two transmitter position candidates/ RC regions in SA, RAML method is better at choosing the right one. It can also be noted that the 5th and 6th reflectors worsen the accuracy of RAML. Those reflectors are the door wall and the window wall. Door wall is highly uneven, while the windows have anti-burglary grilles, causing additional strong reflections not directly from the window.

In the fifth, final, case, RAML method was tested using corridor measurements with receivers at the opposite ends of the corridor. Results are presented in Fig. 20. First of all, the DS method's accuracy is very bad in this case. This is caused by the three receivers being nearly collinear, a geometry strongly damaging to the precision of positioning. Secondly, RAML method's accuracy is better than AH method's. This is again caused by the presence of two transmitter position candidates/ RC regions in the SA, although those are much closer together, given the shape of the SA.

In summary, RAML method has advantages in two cases. First, RAML method is better than the standard AH method in non-cluttered environments. Secondly, RAML method is good at choosing the right transmitter position/position region, making it better than AH method if two transmitter position candidates/ RC regions are in the SA. However, RAML method is worse than AH in cluttered environments with no two possible positions problem.

VI. Conclusions

Using the results of a measurement campaign, we verified the RAML positioning method in three different environments and two receiver placements. The method performs best in the case of not too cluttered rooms. However, even in the case of very cluttered rooms, it can be successfully used to distinguish between two transmitter postion candidates, achieving higher accuracy than the conventional Assumed

Height method. Consequently. the method can be used to increase accuracy of low-density positioning systems as well as a backup in higher receiver density systems.

REFERENCES

[1] J. Kietlinski-Zaleski, T. Yamazato, and M. Katayama, "Experimental validation of toa uwb positioning with two receivers using known indoor features," in *Proc. IEEE/ION Position, Location and Navigation Symposium PLANS 2010*, 2010.

[2] Z. Sahinoglu, S. Gezici, and I. Guvenc, *Ultra-wideband positioning systems: theoretical limits, ranging algorithms, and protocols*. Cambridge Univ Press, 2008.

[3] S. Gezici, Z. Tian, G. B. Giannakis, H. Kobayashi, A. F. Molisch, H. V. Poor, and Z. Sahinoglu, "Localization via ultra-wideband radios: a look at positioning aspects for future sensor networks," *IEEE Signal Process. Mag.*, vol. 22, no. 4, pp. 70–84, July 2005.

[4] J. Schroeder, S. Galler, K. Kyamakya, and T. Kaiser, "Three-dimensional indoor localization in non line of sight uwb channels," in *Proc. IEEE International Conference on Ultra-Wideband ICUWB 2007*, 2007, pp. 89–93.

[5] K. Siwiak, H. Bertoni, and S. M. Yano, "Relation between multipath and wave propagation attenuation," *Electronics Letters*, vol. 39, no. 1, pp. 142–143, 9 Jan 2003.